Textile integrated sensors and actuators for near-infrared spectroscopy

Zysset, Christoph ; Nasseri, Nassim ; Büthe, Lars ; Münzenrieder, Niko ; Kinkeldei, Thomas ; Petti, Luisa ; Kleiser, Stefan ; Salvatore, Giovanni A ; Wolf, Martin ; Tröster, Gerhard

Abstract: Being the closest layer to our body, textiles provide an ideal platform for integrating sensors and actuators to monitor physiological signals. We used a woven textile to integrate photodiodes and light emitting diodes. LEDs and photodiodes enable near-infrared spectroscopy (NIRS) systems to monitor arterial oxygen saturation and oxygenated and deoxygenated hemoglobin in human tissue. Photodiodes and LEDs are mounted on flexible plastic strips with widths of 4 mm and 2 mm, respectively. The strips are woven during the textile fabrication process in weft direction and interconnected with copper wires with a diameter of 71 m in warp direction. The sensor textile is applied to measure the pulse waves in the fingertip and the changes in oxygenated and deoxygenated hemoglobin during a venous occlusion at the calf. The system has a signal-to-noise ratio of more than 70 dB and a system drift of 0.37% ± 0.48%. The presented work demonstrates the feasibility of integrating photodiodes and LEDs into woven textiles, a step towards wearable health monitoring devices.

DOI: https://doi.org/10.1364/OE.21.003213

Textile integrated sensors and actuators for near-infrared spectroscopy

Christoph Zysset,[1,*] Nassim Nasseri,[2] Lars Büthe,[1] Niko Münzenrieder,[1] Thomas Kinkeldei,[1] Luisa Petti,[1] Stefan Kleiser,[2] Giovanni A. Salvatore,[1] Martin Wolf, [2] and Gerhard Tröster [1]

[1]*Electronics Laboratory, Swiss Federal Institute of Technology, Gloriastrasse 35, 8092 Zürich, Switzerland*
[2]*Biomedical Optics Research Laboratory, Division of Neonatology, University Hospital of Zürich 8091 Zürich, Switzerland*
[*]*zysset@ife.ee.ethz.ch*

Abstract: Being the closest layer to our body, textiles provide an ideal platform for integrating sensors and actuators to monitor physiological signals. We used a woven textile to integrate photodiodes and light emitting diodes. LEDs and photodiodes enable near-infrared spectroscopy (NIRS) systems to monitor arterial oxygen saturation and oxygenated and deoxygenated hemoglobin in human tissue. Photodiodes and LEDs are mounted on flexible plastic strips with widths of 4 mm and 2 mm, respectively. The strips are woven during the textile fabrication process in weft direction and interconnected with copper wires with a diameter of 71 µm in warp direction. The sensor textile is applied to measure the pulse waves in the fingertip and the changes in oxygenated and deoxygenated hemoglobin during a venous occlusion at the calf. The system has a signal-to-noise ratio of more than 70 dB and a system drift of 0.37% ± 0.48%. The presented work demonstrates the feasibility of integrating photodiodes and LEDs into woven textiles, a step towards wearable health monitoring devices.

OCIS codes: (170.1460) Blood gas monitoring; (170.3890) Medical optics instrumentation; (170.6510) Spectroscopy, tissue diagnostics.

References and links

1. M. Suh, K. Carroll, and N. Cassill, "Critical Review on Smart Clothing Product Development," J. Text. .Apparel Technol. Manage. **6**, 1–18 (2010).
2. H. Harms, O. Amft, G. Tröster, and D. Roggen, "Smash: A distributed sensing and processing garment for the classification of upper body postures," in *Proceedings of the ICST 3rd Int. Conf. on Body Area Networks,* (Institute for Computer Sciences, Social-Informatics and Telecommunications Engineering, Brussels, 2008), 22:1–22:8.
3. L. van Langenhove and C. Hertleer, "Smart clothing: a new life," Int. J. Clothing Sci. Technol. **16**(1/2), 63–72 (2004).
4. J. W. Zheng, Z. B. Zhang, T. H. Wu, and Y. Zhang, "A wearable mobihealth care system supporting real-time diagnosis and alarm," Med. Biol. Eng. Comput. **45**(9), 877–885 (2007).
5. C. Mattmann, O. Amft, H. Harms, G. Tröster, and F. Clemens, "Recognizing upper body postures using textile strain sensors," in *Proceedings of the 11th International Symposium on Wearable Computers*, (Institute of Electrical and Electronics Engineers, New York, 2007), 29–36.
6. S. Park, K. Mackenzie, and S. Jayaraman, "The wearable motherboard: A framework for personalized mobile information processing (PMIP)," in *Proceedings of the 39th annual Design Automation Conf.* (Association for Computing Machinery, New York, 2002), 174.
7. I. Locher and G. Tröster, "Fundamental building blocks for circuits on textiles," IEEE Trans. Adv. Packag. **30**(3), 541–550 (2007).
8. T. Martin, M. Jones, J. Chong, M. Quirk, K. Baumann, and L. Passauer, "Design and implementation of an electronic textile jumpsuit" in *Proceedings of the 13th International Symposium on Wearable Computers*, (Institute of Electrical and Electronics Engineers, New York, 2009), 157–158.
9. I. Locher and G. Tröster, "Screen-printed textile transmission lines," Text. Res. J. **77**(11), 837–842 (2007).
10. T. Linz, L. Gourmelon, and G. Langereis, "Contacless EMG sensors embroidered onto textile," in *Proceedings of the 4th Int. Workshop on Wearable and Implantable Body Sensor Networks,* (Springer, 2007), 29–34.

#180667 - $15.00 USD Received 27 Nov 2012; revised 23 Jan 2013; accepted 28 Jan 2013; published 1 Feb 2013

11. Y. Kim, H. Kim, and H. Yoo, "Electrical characterization of screen-printed circuits on the fabric," IEEE Trans. Adv. Packag. **33**, 196–205 (2010).
12. C. Zysset, K. Cherenack, T. Kinkeldei, and G. Tröster, "Weaving integrated circuits into textiles," in *Proceedings of the 14th International Symposium on Wearable Computers*, (Institute of Electrical and Electronics Engineers, New York, 2010), 1–8.
13. C. Zysset, T. Kinkeldei, N. Münzenrieder, K. Cherenack, and G. Tröster, "Integration Method for Electronics in Woven Textiles," IEEE Trans Compon. Packag. Manuf. Technol. **2**(7), 1107–1117 (2012).
14. T. Hamaoka, K. K. McCully, M. Niwayama, and B. Chance, "The use of muscle near-infrared spectroscopy in sport, health and medical sciences: recent developments," Philos. Trans. R. Soc. London, Ser. A **369**, 4591–4604 (2011).
15. D. Haensse, P. Szabo, D. Brown, J. C. Fauchère, P. Niederer, H. U. Bucher, and M. Wolf, "A new multichannel near infrared spectrophotometry system for functional studies of the brain in adults and neonates," Opt. Express **13**(12), 4525–4538 (2005).
16. D. M. Mancini, L. Bolinger, H. Li, K. Kendrick, B. Chance, and J. R. Wilson, "Validation of near-infrared spectroscopy in humans," J. Appl. Physiol. **77**(6), 2740–2747 (1994).
17. A. D. Edwards, C. Richardson, P. van der Zee, C. Elwell, J. S. Wyatt, M. Cope, D. T. Delpy, and E. O. Reynolds, "Measurement of hemoglobin flow and blood flow by near-infrared spectroscopy," J. Appl. Physiol. **75**(4), 1884–1889 (1993).
18. M. Wolf, U. Wolf, J. H. Choi, R. Gupta, L. P. Safonova, L. A. Paunescu, A. Michalos, and E. Gratton, "Functional frequency-domain near-infrared spectroscopy detects fast neuronal signal in the motor cortex," Neuroimage **17**(4), 1868–1875 (2002).
19. J. M. Murkin and M. Arango, "Near-infrared spectroscopy as an index of brain and tissue oxygenation," Br. J. Anaesth. **103**(Suppl 1), i3–i13 (2009).
20. K. K. Tremper and S. J. Barker, "Pulse oximetry," Anesthesiology **70**(1), 98–108 (1989).
21. H. Owen-Reece, M. Smith, C. E. Elwell, and J. C. Goldstone, "Near infrared spectroscopy," Br. J. Anaesth. **82**(3), 418–426 (1999).
22. M. Rothmaier, B. Selm, S. Spichtig, D. Haensse, and M. Wolf, "Photonic textiles for pulse oximetry," Opt. Express **16**(17), 12973–12986 (2008).
23. A. Afaq, P. S. Montgomery, K. J. Scott, S. M. Blevins, T. L. Whitsett, and A. W. Gardner, "The effect of current cigarette smoking on calf muscle hemoglobin oxygen saturation in patients with intermittent claudication," Vasc. Med. **12**, 167–173 (2007).
24. R. Boushel and C. A. Piantadosi, "Near-infrared spectroscopy for monitoring muscle oxygenation," Acta Physiol. Scand. **168**(4), 615–622 (2000).
25. A. Jubran, "Pulse oximetry," Crit. Care **3**(2), R11–R17 (1999).
26. S. Lloyd-Fox, A. Blasi, and C. E. Elwell, "Illuminating the developing brain: the past, present and future of functional near infrared spectroscopy," Neurosci. Biobehav. Rev. **34**(3), 269–284 (2010).
27. M. Ferrari, L. Mottola, and V. Quaresima, "Principles, techniques, and limitations of near infrared spectroscopy," Can. J. Appl. Physiol. **29**(4), 463–487 (2004).
28. K. K. McCully, L. Landsberg, M. Suarez, M. Hofmann, and J. D. Posner, "Identification of Peripheral Vascular Disease in Elderly Subjects Using Optical Spectroscopy," J. Gerontol. A Biol. Sci. Med. Sci. **52A**(3), B159–B165 (1997).
29. T. Muehlemann, D. Haensse, and M. Wolf, "Wireless miniaturized in-vivo near infrared imaging," Opt. Express **16**(14), 10323–10330 (2008).
30. D. T. Delpy, M. Cope, P. van der Zee, S. Arridge, S. Wray, and J. Wyatt, "Estimation of optical pathlength through tissue from direct time of flight measurement," Phys. Med. Biol. **33**(12), 1433–1442 (1988).
31. J. G. Webster, *Design of Pulse Oximeters* (IOP Bristol 1997).
32. R. Boushel, H. Langberg, J. Olesen, J. Gonzales-Alonzo, J. Bülow, and M. Kjaer, "Monitoring tissue oxygen availability with near infrared spectroscopy (NIRS) in health and disease," Scand. J. Med. Sci. Sports **11**(4), 213–222 (2001).
33. U. Wolf, M. Wolf, J. H. Choi, L. A. Paunescu, A. Michalos, and E. Gratton, "Regional Differences of Hemodynamics and Oxygenation in the Human Calf Muscle Detected with Near-Infrared Spectrophotometry," J. Vasc. Interv. Radiol. **18**(9), 1094–1101 (2007).
34. W. Cui, C. Kumar, and B. Chance, "Experimental study of migration depth for the photons measured at sample surface," in *Optics, Electro-Optics, and Laser Applications in Science and Engineering*, 180–191 (1991).
35. T. L. Wang and C. R. Hung, "Role of tissue oxygen saturation monitoring in diagnosing necrotizing fasciitis of the lower limbs," Ann. Emerg. Med. **44**(3), 222–228 (2004).
36. U. Wolf, M. Wolf, J. H. Choi, L. A. Paunescu, L. P. Safonova, A. Michalos, and E. Gratton, "Mapping of hemodynamics on the human calf with near infrared spectroscopy and the influence of the adipose tissue thickness," Adv. Exp. Med. Biol. **510**, 225–230 (2003).
37. K. J. Kek, R. Kibe, M. Niwayama, N. Kudo, and K. Yamamoto, "Optical imaging instrument for muscle oxygenation based on spatially resolved spectroscopy," Opt. Express **16**(22), 18173–18187 (2008).
38. J. A. Wahr, K. K. Tremper, S. Samra, and D. T. Delpy, "Near-Infrared Spectroscopy: Theory and Applications," J. Cardiothorac. Vasc. Anesth. **10**(3), 406–418 (1996).
39. P. van der Zee, S. R. Arridge, M. Cope, and D. T. Delpy, "The Effect of Optode Positioning on Optical Pathlength in Near Infrared Spectroscopy of Brain," Adv. Exp. Med. Biol. **277**, 79–84 (1990).
40. J. Schumm, S. Axmann, B. Arnrich, and G. Tröster, "Automatic Signal Appraisal for Unobtrusive ECG Measurements," Int. J. Bioelectromagn. **12**, 158–164 (2010).

#180667 - $15.00 USD Received 27 Nov 2012; revised 23 Jan 2013; accepted 28 Jan 2013; published 1 Feb 2013

41. G. Medrano, L. Beckmann, N. Zimmermann, T. Grundmann, T. Gries, and S. Leonhardt, "Bioimpedance Spectroscopy with textile Electrodes for a continuous Monitoring Application," in *4th International Workshop on Wearable and Implantable Body Sensor Networks (BSN 2007)*, 23–28 (2007).

1. Introduction

Smart textiles or electronic textiles describe the functionalization of textile fabrics and garments with electronic devices. Smart textiles are an attractive approach to sense physiological and environmental parameters in proximity to the human body. Application examples of smart textiles cover a wide range of different fields, ranging from sports to health care, rehabilitation and high-risk professions [1–5]. Devices integrated into textiles can offer several advantages, e.g. reduced number of loose connecting wires between sensors and additional electronics and enhanced mobility and comfort for the wearer.

An approach often followed to manufacture smart textiles is to attach printed circuit boards (PCBs) onto textile substrates [6–10]. Attaching PCBs to textile substrates allows the integration of sensors, actuators, microprocessors, data storage units, communication interfaces, etc. To establish interconnections among individual PCBs on textile substrates, several methods are applicable: gluing copper wires onto textiles [2], weaving copper wires into the textile substrate [7, 8], embroidering conductive yarns [9] or screen-printing conductive ink [9, 11]. However, PCBs attached on textile substrates causes a local stiffness within the textile with the same area as the PCB size.

To reduce the stiffness in smart textiles and therefore enhance the comfort for the wearer, we developed an approach based on weaving flexible plastic strips which serve as substrates for electronic devices [12, 13]. Flexible plastic strips equipped with electronics are woven in weft direction into a textile using an industrial narrow fabric loom. During weaving of a textile, the weft direction describes the lateral direction of the textile and the warp direction the longitudinal direction, respectively. In warp direction, conductive threads are integrated to establish interconnections among individual flexible plastic strips. As an example, Fig. 1 shows a textile with flexible plastic strips carrying digital temperature sensors woven in weft direction and interconnected using two conductive threads in warp direction [12].

Smart textiles with integrated electronics and in particular optic devices are of high interest for the near-infrared spectroscopy and imaging (NIRS and NIRI) community. NIRS and NIRI are applied in many clinical applications, using different types of instruments to track oxygenation and blood flow in tissue [14–27]. Many of these applications could profit from textile integrated optic devices, as described in [22].

In this paper, we demonstrate the integration of the light emitting diodes (LEDs) and photodiodes necessary for near-infrared spectroscopy into a woven textile using flexible plastic strips. The resulting textile is first applied as pulse oximeter, which is a versatile tool used for more than 20 years to monitor the arterial oxygen saturation (SpO_2) of biological tissue [20]. Applications of pulse oximeters range from intensive care to anesthesiology and recovery rooms. A pulse oximeter measures the absorption of light of oxygenated and deoxygenated hemoglobin (O_2Hb and HHb) using two different wavelengths in the near-infrared spectrum, predominantly at the subject's fingertip, ear lobe or toe. The signals of both wavelengths have a pulsatile component, caused by each heart beat by the systole and diastole which allows the calculation of the arterial oxygen saturation.

In a second experiment, the textile is applied to measure changes in O_2Hb and HHb at the calf while performing a venous occlusion. In [28] it is demonstrated that measuring O_2Hb and HHb with a NIRS device can be used as an indicator for peripheral vascular disease (PVD).

First, the integration of LEDs and photodiodes into woven textile is described and demonstrated. The resulting textile is characterized in terms of system noise and system drift. The textile integrated NIRS system is used to measure pulse waves at the finger tip and changes in oxygenated and deoxygenated hemoglobin during a venous occlusion at the calf.

#180667 - $15.00 USD Received 27 Nov 2012; revised 23 Jan 2013; accepted 28 Jan 2013; published 1 Feb 2013

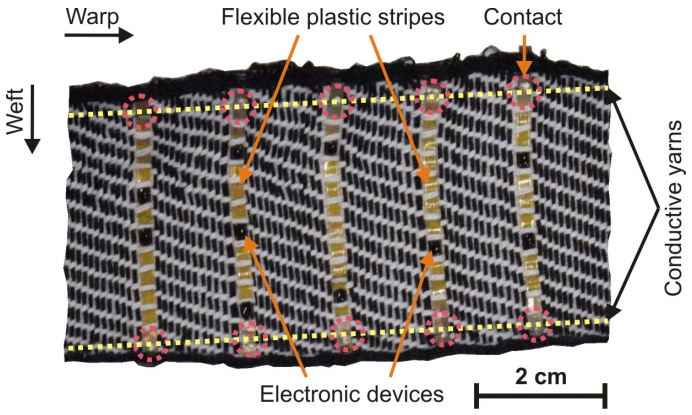

Fig. 1. Smart textile with flexible plastic strips in weft direction and two conductive yarns in warp direction to interconnect electronics on the flexible plastic strips [13].

2. Instrumentation

2.1 Overview

In Fig. 2, a block diagram of the developed system is shown. The system consists of two major building blocks: the sensor textile with LEDs, transistor devices to control the LEDs, photodiodes and transimpedance amplifiers to convert the photocurrent into a voltage. The required devices are mounted on flexible plastic strips which are woven in weft direction and contacted with copper wires in warp direction. The second building block is the control and data acquisition hardware, consisting of a control board with a microcontroller to switch the LEDs on and off and to sample the output voltages of the transimpedance amplifiers. The control board sends the data via a USB connection to a host computer for storage and post processing.

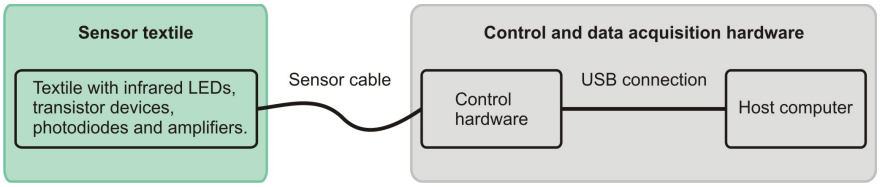

Fig. 2. System overview: the sensor textile incorporates LEDs, transistor devices, photodiodes and transimpedance amplifiers and copper wires to contact the devices. The control and data acquisition hardware controls the LEDs, samples the voltages of the transimpedance amplifiers and sends the data to a host computer for storage and further processing.

2.2 Sensor textile

To integrate the required devices into the sensor textile as shown in Fig. 2, the following concept was applied: LEDs together with transistor devices to control the LEDs were mounted on one strip (LED strip), a photodiode with a transimpedance amplifier on a second strip (photodiode strip) and a third strip was used to connect all the strips within the textile using copper wires (bus bar strip). Figure 3 shows a schematic overview of the system with one bus bar strip, two LED strips and two photodiode strips in weft direction to enable the measurement at two different locations labeled in Fig. 3 as A and B. In warp direction, copper wires interconnect the strips. The distance between the two photodiode strips is approximately 0.5 cm and the distance between a photodiode strip and an LED strip approximately 1.7 cm in accordance with existing NIRS devices [29].

#180667 - $15.00 USD Received 27 Nov 2012; revised 23 Jan 2013; accepted 28 Jan 2013; published 1 Feb 2013

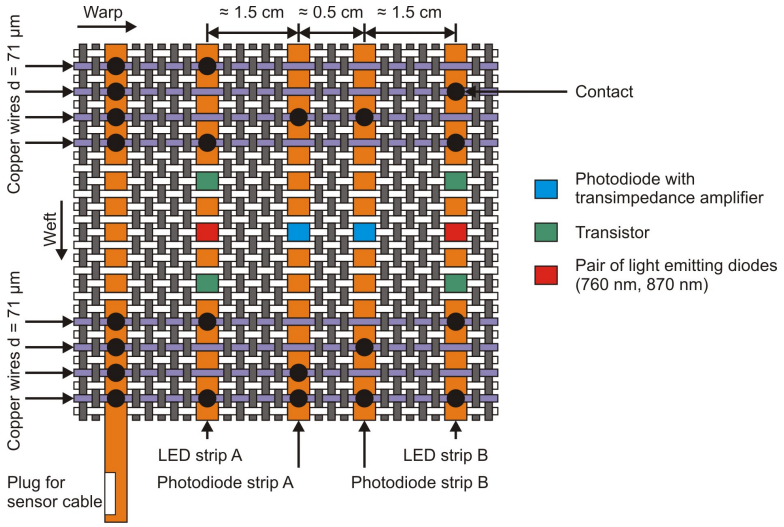

Fig. 3. Schematic of the sensor textile with two photodiode strips, two LED strips and a bus bar strip. The individual strips are connected among each other using copper wires in warp direction.

The three strip types were fabricated using a 2-layer flexible plastic substrate (manufactured by Dyconex AG). The strips had a total thickness of 72 µm (25 µm bottom polyimide, 11 µm sandwiched metal, 25 µm polyimide, and 11 µm top metal).

LEDs, transistor devices, photodiodes and amplifiers were mounted on the flexible strips using standard micro-fabrication techniques such as wire bonding, soldering and gluing:

1. LED strip: two LEDs (Epigap ELC-760-26, size 320 µm by 320 µm, wavelength 760 nm and Epigap ELC-870-17-2, size 360 µm by 360 µm, wavelength 870 nm) were mounted in conjunction with two transistors (FDN357N, size 1.7 mm by 0.76 mm) as bare dies onto the substrate. All devices were encapsulated using intransparent epoxy (Epo-Tek T7139) and transparent epoxy (Epo-Tek 301-2). The strip has a length of 6 cm and a width of 2 mm. Figure 4(a) shows a LED strip with the devices and the contact pads for the copper wires.

2. Photodiode strip: a PIN photodiode with an active area of 7.7 mm^2 (Vishay VBPW34S) was mounted onto the strip together with a bare die amplifier (Texas Instruments TLV2721, size 1.17 mm by 0.79 mm) in a transimpedance amplifier configuration with a feed-back resistor of 100 kΩ. The transimpedance amplifier and the contacts of the photodiode were covered with intransparent epoxy. Figure 4(b) depicts a photodiode strip with a length of 6 cm and a width of 4 mm.

3. Bus bar strip: Fig. 4(c) shows a bus bar strip to route the eight copper wires within the textile to a single plug.

To fabricate the sensor textile, flexible plastic strips were woven into a 4.5 cm wide and approximately 10 cm long textile band using an industrial narrow fabric weaving machine (Müller Frick NFREQ 42, shown in Fig. 5). The weaving machine was prepared by replacing 8 yarns in warp direction with insulated copper wires (71 µm diameter) to interconnect the individual strips as illustrated in Fig. 3. The textile yarns in weft and warp direction were made of cotton.

#180667 - $15.00 USD Received 27 Nov 2012; revised 23 Jan 2013; accepted 28 Jan 2013; published 1 Feb 2013

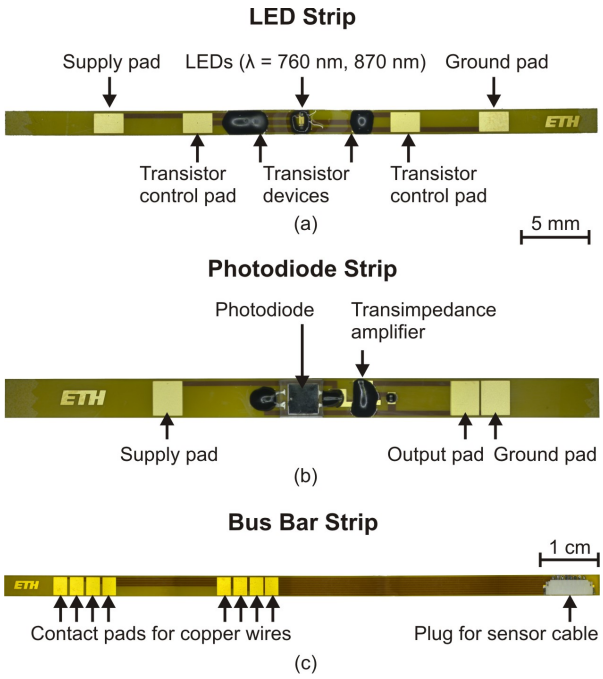

Fig. 4. (a) LED strip with the LED pair at the center and the two transistors on the left and right side of the LED pair. (b) Photodiode strip with photodiode and transimpedance amplifier. (d) Bus bar strip with a plug to connect the sensor textile to the control hardware and the contact pads for the copper wires. In a) and b) the contact pads are indicated.

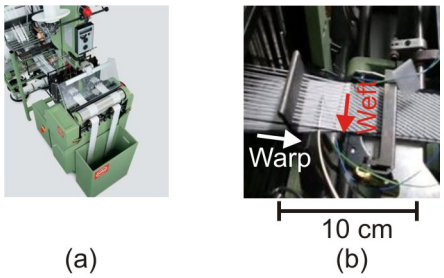

Fig. 5. (a) Narrow fabric weaving machine (Müller Frick NFREQ42) used to weave flexible strips in weft direction into a textile. (b) Yarns in warp and weft direction.

Weaving was performed by blocking the insertion of the weft yarn to open space for a flexible plastic strip, then stopping the machine and manually inserting a strip. Finally, cotton yarns were woven until the next strip was inserted. A detailed description and analysis of weaving flexible plastic strips can be found in [13].

After weaving flexible plastic strips, contacts between insulated copper wires and contact pads on flexible plastic strips were established by locally removing the varnish of the copper wire with a soldering iron, incinerating the varnish. Then, the contact pads and the skinned copper wire were soldered and covered with epoxy (Epo-Tek T7139). Figure 6 shows a photograph of the resulting textile.

To enable measurements on the human body, for example at the calf, the sensor textile was sewn into a textile cuff. Sewn in Velcro strips in the cuff allow attaching the cuff to the leg. Figure 7(a) shows the cuff with the sewn in sensor textile and the Velcro strips and in Fig. 7(b) the cuff is strapped to a leg together with the control hardware.

#180667 - $15.00 USD Received 27 Nov 2012; revised 23 Jan 2013; accepted 28 Jan 2013; published 1 Feb 2013

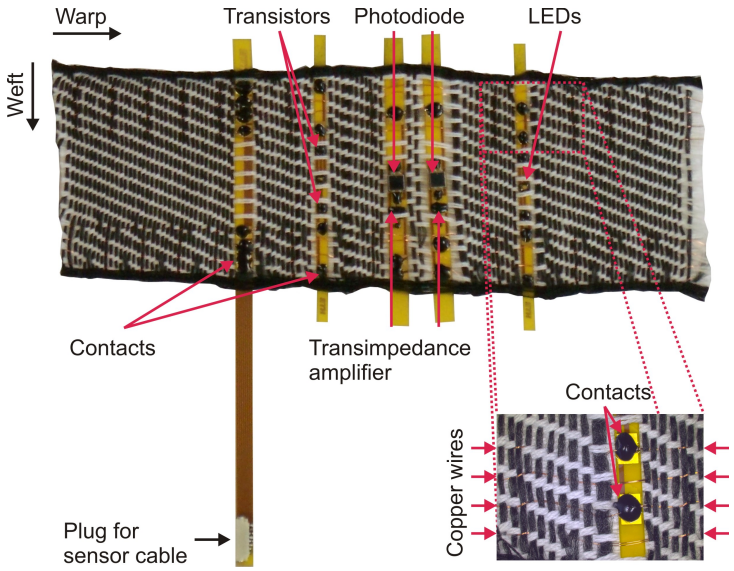

Fig. 6. Woven sensor textile with flexible plastic strips in weft direction carrying LEDs, transistors, photodiodes and transimpedance amplifiers. In the inset, woven copper wires in warp direction are visible together with two encapsulated contacts between copper wires and contact pads on a flexible strip.

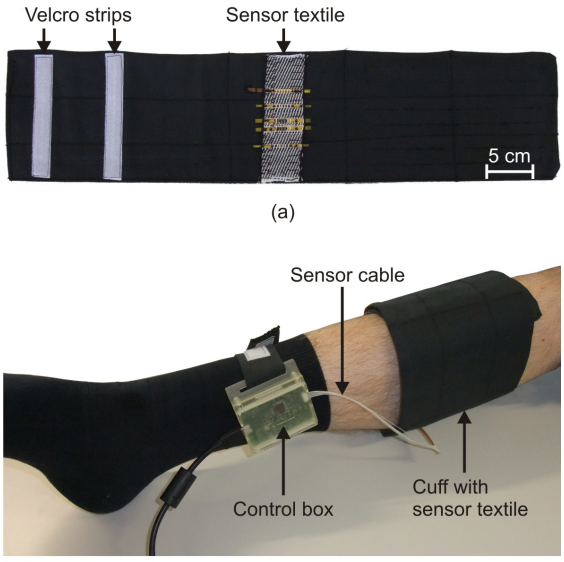

Fig. 7. In (a) the sensor textile is sewn into a textile cuff together with Velcro strips for attaching to the human body. (b) The cuff is strapped to the calf together with the control box. Between the control box and the cuff, the sensor cable is visible.

2.3 Control and data acquisition hardware

The control and data acquisition hardware manages the timing of the LEDs, samples the output voltages of the transimpedance amplifiers and stores the collected data on a host computer.

To measure the light intensity of each LED individually, the LEDs were controlled in a time-multiplexed fashion with a 10 ms measurement cycle corresponding to a sampling rate

#180667 - $15.00 USD Received 27 Nov 2012; revised 23 Jan 2013; accepted 28 Jan 2013; published 1 Feb 2013

of 100 Hz. Within the 10 ms measurement cycle, each of the four LEDs (two LED strips, each having two LEDs) is switched on for 1 ms. In-between the on states of the individual LEDs, all LEDs are turned off for 1.5 ms. The timing sequence is shown in Fig. 8. The photodiodes are sampled 64 times with a 10-bit ADC within a time slot of 250 µs during the on state of the LEDs and once in the off state of all LEDs to measure the background signal.

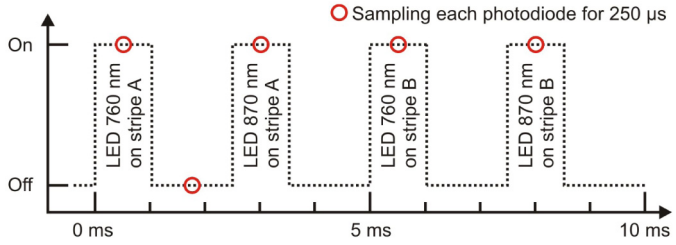

Fig. 8. Timing of the LEDs in the sensor textile. The circles indicate the sampling of each photodiode for 250 µs.

3. Experiments and results

First, experiments were performed to assess the system noise and the system drift. Subsequently, the textile was used to measure the pulse wave in a fingertip and extracting the arterial oxygen saturation (SpO_2) from the measurement. Finally, the textile was strapped to the calf of a volunteer and the changes in O_2Hb and HHb concentration were monitored during a venous occlusion.

3.1 System noise

System noise was evaluated by laying the sensor textile on a flat surface and placing a phantom material on top. The phantom consisted of a transparent (in the near infrared wavelength region) silicone rubber with a scatterer (μ_s = 13 cm^{-1}) and an absorber (μ_a = 0.09 cm^{-1}). The system was run for 15 minutes with a sample rate of 100 Hz. The system noise was determined as the standard deviation of the light intensity at the photodiode within each block of 10 samples. The resulting noise is expressed as percentage of the mean light intensity at the photodiode within the corresponding block of 10 samples, according to the method in [15].

In Tab. 1, the system noise is given as mean and standard deviation calculated over all blocks of 10 samples. The measured values correspond to a signal-to-noise ratio of at least 70 dB.

Table 1. System Noise: Mean Over All Standard Deviations Calculated from Blocks of 10 Samples Recorded with a Sampling Rate of 100 Hz for a Time Period of 15 Minutes

Wavelength	760 nm	870 nm
Noise ± Standard deviation	0.012% ± 0.0096%	0.0083% ± 0.0053%

3.2 System drift

Self-heating of the system due to current flow in resistors can cause a drift in the sensor values. Therefore, the drift of the sensor signals was calculated for 15 minutes after system start up with the phantom medium as scatterer and absorber. The measurement was performed with a sampling rate of 100 Hz. In Tab. 2, the signal drifts for both wavelengths are given for intervals of 1 minute. Within the 1 minute intervals, the change between the mean light intensity at the photodetector of the first 10 samples and the last 10 samples was compared and expressed as a percentage of the mean light intensity of the first 10 samples.

In the first minute, the signals drifted by 3.5%, whereas in the second minute the system drifted by 1% and from the third minute on, signal drift was less than 0.6%.

#180667 - $15.00 USD Received 27 Nov 2012; revised 23 Jan 2013; accepted 28 Jan 2013; published 1 Feb 2013

Table 2. Signal Drift for Both Wavelengths after System Start Up[a]

Wavelength	760 nm	870 nm
Minute 1	2.8%	3.5%
Minute 2	0.8%	0.9%
Minutes 3-15 *Mean* ± *SD*	0.29% ± 0.26%	0.14% ± 0.12%

[a]For each minute, the change was calculated from the last sample with regards to the first sample of the corresponding minute.

3.3 Pulse wave measurement

As a preliminary test to monitor the functionality of the system, pulse waves were measured to detect the heart rate. To measure pulse waves in arterial blood, a fingertip was placed on the LEDs and photodiodes. Data was acquired with a sample rate of 100 Hz. In Fig. 9 recorded data of pulse waves are shown in ADC values for both wavelengths (760 nm and 870 nm). The pulsation is caused by every heart beat with systole and diastole. Within the 20 s period, 25 peaks are detected corresponding to a heart rate of 75 bpm, which was confirmed by palpating the radial artery.

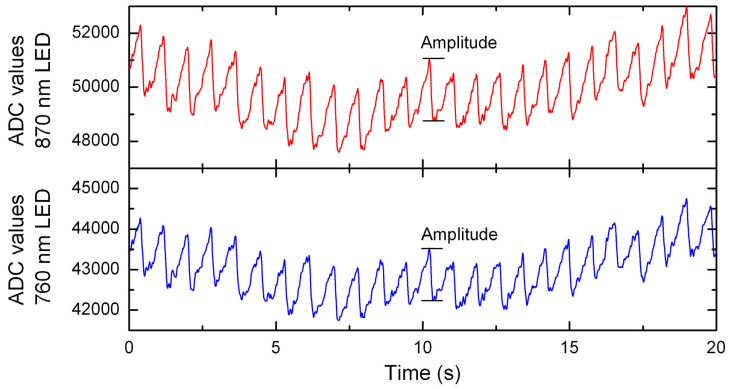

Fig. 9. Pulse waves recorded at the fingertip. In the 20 s period, 25 peaks are detected corresponding to a heart rate of 75 bpm. The maximum ADC value is 65472 (sum of 64 samples of a 10-bit ADC).

3.4 Arterial oxygen saturation SpO_2

To calculate arterial oxygen saturation (SpO_2) the following procedure was followed: first, the natural logarithm of the light intensities at the photodiode was taken, leading to the light attenuations A_{760nm} and A_{830nm}, respectively. Then, the values for A_{760nm} and A_{830nm} were high-pass filtered to remove the baseline (slowly varying part of the signal in Fig. 9), because for SpO_2 only the pulsating part, denoted as amplitude in Fig. 9 is of interest. The modified Beer-Lambert law [30] allows the calculation of changes in oxygenated (O_2Hb) and deoxygenated hemoglobin (HHb) using the following equations:

$$\Delta HHb \cdot d \cdot DPF = -0.3557\Delta A_{760nm} + 0.1959\Delta A_{870nm} \quad (1)$$

$$\Delta O_2Hb \cdot d \cdot DPF = 0.2469\Delta A_{760nm} - 0.5066\Delta A_{870nm} \quad (2)$$

where d denotes the distance between light source and detector and DPF the differential pathlength factor, which takes the prolonged light path in the tissue due to multiple scattering into account.

To compute the change of $\Delta HHb \cdot d \cdot DPF$ and $\Delta O_2Hb \cdot d \cdot DPF$ in the arterial blood over time, the standard deviation of $\Delta HHb \cdot d \cdot DPF$ and $\Delta O_2Hb \cdot d \cdot DPF$ was calculated. The standard deviation of $\Delta HHb \cdot d \cdot DPF$ and $\Delta O_2Hb \cdot d \cdot DPF$ is sufficient to calculate SpO_2. This is because SpO_2 is determined as a ratio and therefore the proportionality factor which relates the

#180667 - $15.00 USD Received 27 Nov 2012; revised 23 Jan 2013; accepted 28 Jan 2013; published 1 Feb 2013

standard deviations σ of ΔHHb·d·DPF and ΔO_2Hb·d·DPF to the amplitude of ΔHHb·d·DPF and ΔO_2Hb·d·DPF is canceled out, as well as d and DPF:

$$SpO_2(\%) = \frac{\Delta O_2 Hb \cdot d \cdot DPF}{std\,\Delta O_2 Hb \cdot d \cdot DPF + \Delta HHb \cdot d \cdot DPF} \cdot 100 \tag{3}$$

$$SpO_2(\%) = \frac{\Delta O_2 Hb}{\Delta O_2 Hb + \Delta HHb} \cdot 100 = \frac{\sigma(\Delta O_2 Hb)}{\sigma(\Delta O_2 Hb) + \sigma(\Delta HHb)} \cdot 100 \tag{4}$$

SpO_2 was calculated for segments of 5 seconds (500 samples) using a sliding window with a width of 2.5 seconds (250 samples).

In Fig. 10, an exemplary segment of data and the corresponding SpO_2 values are given. The calculations yielded a SpO_2 value of 94.1% ± 0.4% which is in agreement with standard pulse oximetry data [31]. For practical applications for example in clinics, a smoothing algorithm (i.e. median filter) for the SpO_2 curve in Fig. 8 can be of use to obtain less varying values.

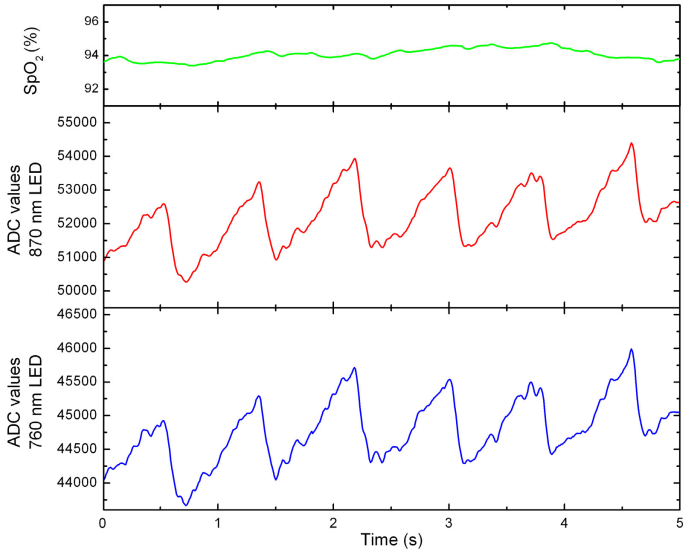

Fig. 10. Pulse waves and their calculated SpO_2 value.

3.4 Venous occlusion

The following procedure was applied for the venous occlusions: the textile cuff with the integrated sensor textile was attached to the calf as shown in Fig. 7(b). After the system was turned on, 2 minutes of data was recorded as baseline. Then, a venous occlusion was performed by inflating a pressure cuff around the thigh to 60 mmHg. The occlusion was kept for 2 minutes. Finally, pressure was released from the cuff to allow a normal blood circulation. From the recorded light intensities, ΔHHb, ΔO_2Hb, change in total hemoglobin tHb and tissue oxygen saturation StO_2 was calculated [15]. In Fig. 11, an exemplary measurement result is shown, with the occlusion period marked in grey.

#180667 - $15.00 USD Received 27 Nov 2012; revised 23 Jan 2013; accepted 28 Jan 2013; published 1 Feb 2013

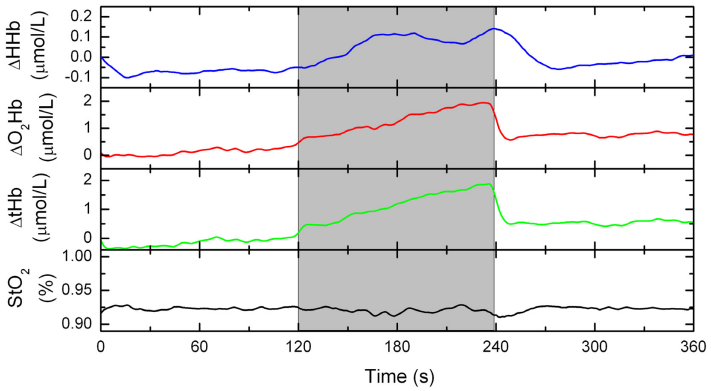

Fig. 11. Venous occlusions were performed on the calf for 2 minutes (marked in grey). During the occlusion, the HHb, O_2Hb and tHb concentrations did increase while the tissue oxygen saturation StO_2 stayed constant.

The changes in HHb (+ 0.2 µmol/L), O_2Hb (+ 1.5 µmol/L) and tHb (+ 1.7 µmol/L) are in agreement with published data for venous occlusions [17, 32, 33]. However, it is to note that the changes in HHb, O_2Hb and tHb are by trend smaller than the average values given in [33]. The smaller values arise from the different source/detector spacing used in this study (17 mm short distance between source and detector and 22 mm long distance, cf. Figure 3) and in [33] where the spacing was between 24 mm and 35 mm. An increased spacing between source and detector allows a deeper penetration of the infrared light into the tissue and therefore more light absorption in the muscles [34]. The average StO_2 value of 92% is within the StO_2 range of 82% ± 17% reported in [35] for lower legs obtained with an source/detector spacing of 20 mm. The venous oxygen saturation SvO_2 was 88%, which is again somewhat higher than the value of 77.6% ± 5.9% [33]. Our setup is more sensitive to the adipose tissue layer, which has a smaller light absorption, and by its nature a higher oxygenation [36], which explains our results. To increase the reliability of StO_2 and SvO_2 measurements [37], suggests source/detector spacing larger 20 mm to reduce the influence of the skin and the adipose tissue layer.

3.5 Influence of source/detector distance change

The textile integration of the LEDs and photodetectors leads to an unstable geometry between source and detector which changes the distance between LEDs and photodetectors. Despite the usage of cotton yarns for the woven textile which are not stretchable, the source/detector distance can vary by approximately ± 2 mm due to the flexibility of the textile. Equations (1) and (2) show the dependency of HHb and O_2Hb on the source/detector distance. Therefore, the occlusion data was evaluated taking the distance variation into account. The result is depicted in Fig. 12, where the solid line represents the calculated changes in HHb and O_2Hb with the initial distance (17 mm short source/detector distance, 22 mm long source/detector distance) and the dashed lines the changes in HHb and O_2Hb with the initial distance ± 2 mm. The calculations show that HHb is tainted with an uncertainty of ± 0.08 µmol/L and O_2Hb with ± 0.2 µmol/L for this particular measurement. It is to note that the possible variation of the source/detector distance should be taken into account for each measurement, leading to an uncertainty range around the curves for HHb and O_2Hb concentrations obtained with the initial source/detector spacing.

4. Conclusion

In this report, a textile with integrated LEDs, transistors, photodiodes and transimpedance amplifiers was presented. The textile integration method based on flexible plastic strips which served as carriers for the electronic devices. A narrow fabric weaving machine was applied to integrate the flexible plastic strips in weft direction into a woven textile during the weaving

#180667 - $15.00 USD Received 27 Nov 2012; revised 23 Jan 2013; accepted 28 Jan 2013; published 1 Feb 2013

process. In warp direction, copper wires were woven to establish connections among flexible plastic strips.

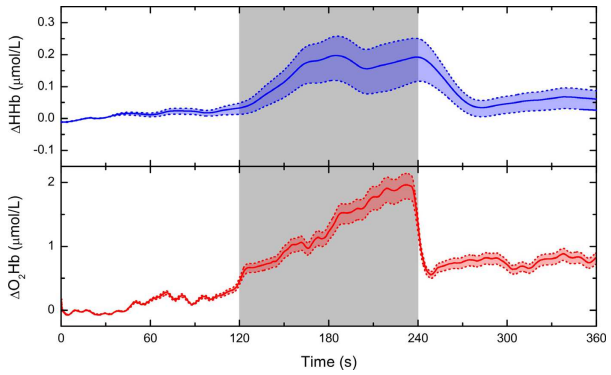

Fig. 12. Changes in HHb and O_2Hb during a venous occlusion, taking the source/detector distance variation of ± 2 mm into account. The solid lines represent the HHb and O_2Hb changes with the initial distance of 17 mm short distance and 22 mm long distance, and the dashed lines the initial distance ± 2 mm.

The resulting textile was characterized with respect to drift and system noise. The measurements showed a drift of the intensity signals for both wavelengths of up to 3.5% within the first two minutes after system start up. After the second minute signal drift evaluated within intervals of 1 minute was 0.29% ± 0.26%. The signal-to-noise ratio of the system was determined to be at least 70 dB.

Placing a fingertip on a photodiode and a pair of LEDs allowed to measure pulse waves in arterial blood. A heart rate of approximately 75 bpm was extracted and confirmed by palpating the pulse at the wrist. In addition, the pulse waves could be used to extract the arterial oxygen saturation SpO_2 via the amplitudes of oxygenated and deoxygenated hemoglobin, which was in the presented example 94.1% with a standard deviation of 0.4%.

The obtained results for the occlusion measurement show that it is possible to detect changes in HHb and O_2Hb caused by a venous occlusion. However, textile integration of sensors and actuators influences the NIRS measurements, especially with regards to known limitations of NIRS systems, such as distance variation between source and detector or motion artifacts [38, 39]. For the textile integrated NIRS system, the distance between LED and photodiode can vary due to the flexibility of the textile and should be taken into account during data analysis and interpretation. Motion artifacts can change the locations of the LED and detector on the skin. Such effects influencing the signal quality are commonly observed with textile integrated sensor systems for physiological signals. Examples are demonstrated for ECG measurements [3, 40] and bio-impedance measurements [41].

Nevertheless, the presented NIRS system in this paper is a step towards textile integration of NIRS systems enabling long term monitoring. Integrating sensors and actuators for near-infrared spectroscopy into woven textiles using flexible plastic strips offers the advantage of mechanically flexible sensor systems. Therefore, the sensor textile is adaptable to individual users with different shapes of for example their calves. In addition, textile integrated sensor systems promise the possibility of long-term monitoring of patients due to the increased comfort. This is potentially interesting for diabetes patients and smokers who can suffer from peripheral vascular diseases.

Acknowledgment

This project was financed with a grant from the Swiss Nano-Tera initiative and evaluated by the Swiss National Science Foundation. The authors would like to thank Sabine Nicoli and Yasmin Egli from the Swiss Textile College, Martin Lanz from the Swiss Federal Institute of Technology Zurich and Andreas Jakko Metz from the University Hospital of Zurich.

#180667 - $15.00 USD Received 27 Nov 2012; revised 23 Jan 2013; accepted 28 Jan 2013; published 1 Feb 2013